ARTICLE

Measurement of Electron Affinity of Atomic Lutetium via the Cryo-SEVI Method†

Xiao-xi Fu[a], Ru-lin Tang[a], Yu-zhu Lu[a], Chuan-gang Ning[a,b]*

a. Department of Physics, State Key Laboratory of Low-Dimensional Quantum Physics, Tsinghua University, Beijing 10084, China
b. Collaborative Innovation Center of Quantum Matter, Beijing 100084, China

(Dated: Received on December 27, 2018; Accepted on January 22, 2019)

Electron affinities (EAs) of most lanthanide elements still remain unknown due to their relatively low EA values. In the present work, the cryogenically controlled ion trap is used for accumulating atomic lutetium anion Lu^-, which makes the measurement of electron affinity of lutetium become practicable. The high-resolution photoelectron spectra of Lu^- are obtained via the slow-electron velocity-map imaging method. The electron affinity of Lu is determined to be 1926.2(50) cm^{-1} or 0.23882(62) eV. In addition, two excited states of Lu^- are observed.

Key words: Electron affinity, Cryogenically controlled ion trap, Lutetium anion

I. INTRODUCTION

Experimental investigations of negative ions provide a unique method for shedding light on many-body problems. Negative ions are distinct from their neutral counterparts and the positive ions in that the extra electron is bound to the remaining core via the short-range force rather than Coulomb binding force. Negative ions usually only have a few bound states due to the short-range force. Thus it cannot be more preferable to study electron-electron correlation effects and core polarizations through negative ions [1]. As for the theoretical side, many effects ignored in neutral atoms have to be taken into account when calculating the binding energies of even the simplest anionic systems. The influences of electron correlation effects and relativistic effects add much more difficulties in calculations for heavy elements, especially for lanthanides due to the partially filled d- or f-type orbitals [2, 3]. Thus it is indispensable to conduct experiments to test the validity of computational approximations [1–6].

Electron affinity (EA), one of the fundamental parameters of atoms, is defined as the energy difference between the negative ion and the corresponding neutral atom (both in their ground states) [6]. EAs of most lanthanide elements are still unknown due to the practical difficulties in measuring EA values via traditional methods [2, 3]. Firstly, generating stable and considerably strong ion beams of lanthanides is not an easy task. The oxide and hydride anions are unintendedly dominant in mass spectra. Signals of atomic anions are usually extremely weak [7, 8]. Secondly, the relative low EAs of lanthanides, typically about 0.2 eV, bring out the necessity of far infrared light sources when using traditional methods, which are nevertheless scarce. Thirdly, atomic anions of lanthanides usually have several bound states, and their electronic structures of neutral atoms are very complicated. These cause very congested spectra which cannot be well resolved by traditional methods. Moreover, the theoretical predictions of electronic structures and binding energies for lanthanides still remain challenging [1–6].

In 2001, Davis and Thompson reported the experimental work for measuring EA value of Lu for the first time by using the laser photodetachment electron spectroscopy technique [9]. EA of Lu was determined to be (0.34±0.01) eV. They also observed one excited state, and its binding energy was measured as (0.16±0.02) eV. On the theoretical side, several different methods have been reported for predicting the EA value of Lu. Vosko and Chevary reported a value to be (0.19±0.11) eV via the DFT-HF calculations [10]. They also predicted that Lu^- was stable in the $[Xe]4f^{14}5d^16s^26p^1$ odd-parity electron configuration instead of $[Xe]4f^{14}5d^26s^2$ even-parity configuration. The relativistic Fock-space coupled-cluster method was employed by Eliav *et al.* and two bound states of Lu^-, $6p5d\ ^1D_2$ and $6p^2\ ^3P_0$, were predicted with binding energies of about 2100 and 750 cm^{-1} respectively [11]. Borschevsky *et al.* calculated the EA of Lu to be 2706 cm^{-1} by the intermediate Hamiltonian coupled cluster method [12]. Two more bound states $^3D_2$ and $^3P_0$ were predicted. The method within the frame work of the Breit-Pauli Hamiltonian and the relativistic Hartree-Fock method was adopted

†Part of the special issue for "the 19th International Symposium on Small Particles and Inorganic Clusters"
*Author to whom correspondence should be addressed. E-mail: ningcg@tsinghua.edu.cn

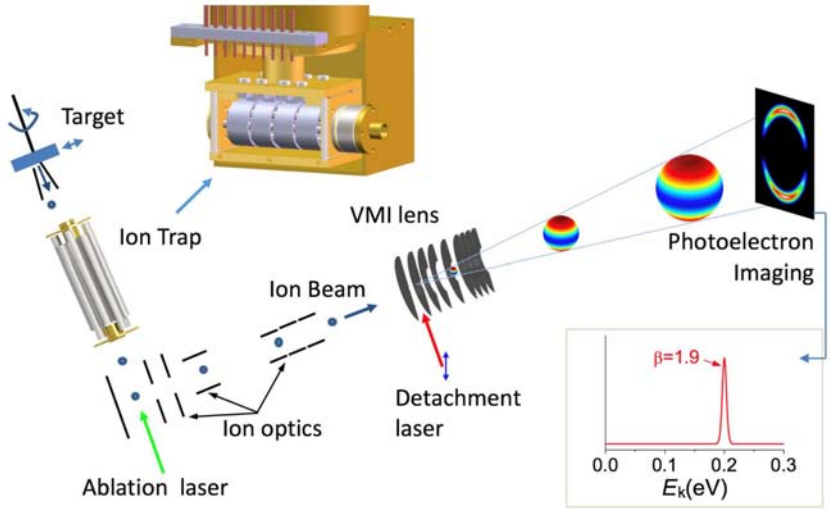

FIG. 1 Schematic view of the experimental setup. A mass gate and a rotatable ion detector in front of the VMI lens are not shown. The inset at the bottom right corner shows the photoelectron spectrum reconstructed from the projected image.

by Karaçoban and Özdemir. EA was predicted to be 2665 cm^{-1} [13]. O'Malley and Beck predicted the EA of Lu to be 329 meV using valence shell relativistic configuration interaction calculations [14]. Later they revised the value to be 353 meV considering their "complete calculations" [15].

In the present work, the combination of the cryogenically controlled ion trap [16, 17] and the slow-electron velocity-map imaging method [18–20] (Cryo-SEVI) was used to measure the EA of atomic Lu. The SEVI method had very impressive energy resolution of a few cm^{-1} and guaranteed signal intensities for low-energy electrons [18, 19, 21–23]. In our previous work, we have improved the uncertainties of EAs of several transition elements to the accuracy of ∼0.5 cm^{-1} via this method [24–31]. As demonstrated in our recent work for EA measurement of titanium [27], the cryogenically ion trap can effectively enhance the intensity of negative ions through accumulations. It should be mentioned that the trace water or oxygen condensate completely in the cold ion trap, which is important for trapping the reactive anions. Moreover, the ability to reduce thermal broadening and hot bands is crucial for obtaining a clean and sharp spectrum for molecular anions, which might be the most important advantage of a cold ion trap.

II. EXPERIMENTS

Our cryo-SEVI apparatus have been described in detail previously [27]. Targeted anions are produced, trapped, mass-selected, and finally photodetached by a tunable laser. The kinetic energies of injected photoelectrons (E_k) are measured through a velocity-map imaging (VMI) spectrometer [19, 32]. The binding energies (BE) are deduced from the energy conservation, BE=$h\nu-E_k$. Here $h\nu$ is the photon energy.

Anions were generated by a laser ablation ion source. A 532 nm pulse radiation of about 10 mJ from an Nd:YAG laser working at a 20 repetition rate was aimed onto the surface of a lutetium disk. The disk was designed to be translating as well as rotating so that the entire surface would not be worn out quickly. The formed plasma flew through an Einzel lens and was guided to an ion trap held at a variable temperature of 5−300 K mounted on the second stage of a liquid helium refrigerator. In order to isolate the ion trap from the thermal exchange with the surrounding environment, a 40-K copper shield was connected with the first stage of the refrigerator. While stored in the trap for about 40 ms, the trapped ions lost kinetic energies through collisions with a mixture of H_2 and He buffer gases (20:80). As shown in FIG. 1, two electrodes at the entrance and the exit of the ion trap confined the ions axially and the linear RF octupole confined them radially. The trapped ions can be ejected out tightly with the help of the four ring electrodes.

The extracted ions were accelerated by a −1000 V high-voltage pulse in the Wiley-McLaren time-of-flight mass spectrometer [33]. Then, they were detected by an ion detector, which is composed of a pair of microplates. The ion detector could be rotated out of the ion flight path for the following photodetachment experiment. The typical mass resolution ($m/\Delta m$) is 1000 for m≈200. Finally, the ions of interest were picked out via a mass gate and headed into the interaction region of the VMI lens, where they were photodetached by a Nd:YAG-pumped tunable dye laser. The outgoing photoelectrons were proliferated by two chevron-stacked microchannel plates and imaged on a coupled phosphor screen. The raw photoelectron images were recorded by a CCD camera for each laser shot in real time.

DOI:10.1063/1674-0068/cjcp1812293

Event-counting software was applied to find the hitting position of each photoelectron. A typical photoelectron image was an accumulated result of 50000 laser shots. The wavelength of the dye laser was monitored in real time by a HighFinesse WS-600 wavelength meter with an accuracy of 0.02 cm^{-1}. The polarization vector of the detachment laser was parallel to the phosphor screen. Hence the raw image had a cylindrical symmetry. The maximum-entropy velocity Lengendre method was used to reconstruct the radial and angular distributions from the accumulated images in this work [34]. Velocities of photoelectrons were proportional to the measured radii r of the rings in the image.

For one-photon detachment, the photoelectron angular distribution (PAD) is given by the expression [35, 36]

$$I(\theta) = \frac{\sigma}{4\pi}[1 + \beta P_2(\cos\theta)] \quad (1)$$

Here θ is the angle of the outgoing electron relative to the laser polarization and P_2 is the second-order Legendre polynomial. σ is the total photodetachment cross section. β is defined as the asymmetry parameter, lying between the values of 2 and -1. The β value depends on eKE and electronic states [36]. As for atomic anions, when the s-orbital electron is photodetached, the outgoing photoelectron is p wave because of the conservation of the angular momentum. The intensity distribution is proportionate to $\cos^2\theta$ and β equals to 2. When the p-orbital electron is photodetached, the outgoing photoelectron is the superposition of s and d partial waves. However, the s-wave is dominant near the threshold due to the centrifugal potential which is proportional to $l(l+1)/r$ for the lth partial wave. Near the threshold, β equals to zero. As the kinetic energy of the ejected electron is increased, the partial waves of s-wave and d-wave both matter. The β value gradually decreases, and reaches the minimum of -1, and then increases if the energy continues to increase. When the d-orbital electron is photodetached, the outgoing photoelectron is the superposition of p and f partial waves. Near the threshold, β is slightly greater than zero. And it will decrease as the kinetic energy increases.

III. RESULTS AND DISCUSSION

FIG. 2 shows the photoelectron image and binding energy spectra obtained at photon energy $h\nu$=11590.36 cm^{-1}. In order to distinguish transitions from different initial states, the trapping time is varied. The shorter the trap time is, the higher the chances that the excited states do survive will be. That is to say, the peak intensities from the excited states will increase as the trapping time decreases. The spectra with trapping time of 45 and 5 ms are plotted together under the condition that the peak g is set to be normalized. The strongest peak g is supposed to be the transition from the ground state of the anions and its intensity

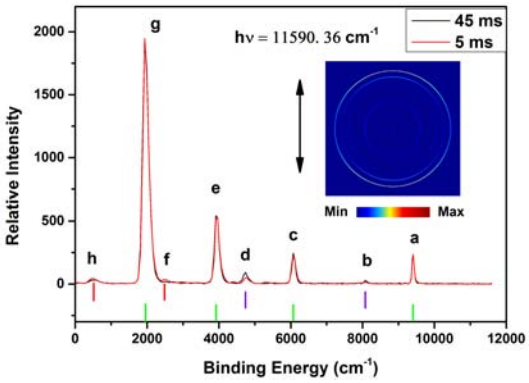

FIG. 2 Comparison of photoelectron spectra of Lu^- with different trapping time. A series of vertical sticks represent the energy levels of neutral atom Lu. The colors of vertical sticks indicate three different bound states of Lu^-. The inset shows the photoelectron image for the trapping time of 45 ms. The double arrow indicates the laser polarization.

can be regarded invariable whatever the trapping time is. Those peaks with the same initial states should follow the same trend as the trap time changes. In this way the relative changes of peak intensities are very helpful for the state assignments.

As mentioned above, we can conclude that peaks g, e, c, and a correspond to transitions from the ground state of Lu^- since their intensities barely change under two trapping conditions. Peaks d and b are assigned to be originated from a common initial state. So do peaks h and f. It is also worth mentioning that energy levels of Lu from the NIST database can be used as fingerprints in the assignment processes of final states [37]. In other words, if two transitions belong to the same initial state, their binding energy difference must equal to that of two energy levels of the neutral atom. As shown in FIG. 2, a series of vertical sticks were plotted to show the coincidences. The relative positions of sticks are the energy levels of Lu. The final states of the transitions sharing the same initial state can be figured out instantly through those vertical sticks. These determinations of final states further confirm our previous conclusions about the peaks with the same initial states. In view of the previous calculation work, the ground state of Lu^- is predicted as $6s^26p5d\ ^1D_2$ [10, 11, 14, 15]. Our experimental results are consistent with this prediction. The terms of final states of peaks g, e, b, and a are ^2D and ^2P [37]. Among the calculated possible terms of the initial state, $^3F_{2,3}$, $^3P_0$ and $^1D_2$, the L quanta tends to be D or P instead of F based on the transition rules [15]. More interestingly, the intensities of peaks d and b are deviated from general features of transitions from excited states. Generally, the shorter the trapping time is, the stronger the peaks for an excited state will be. For example, peaks h and f do become stronger with shorter trapping time of 5 ms. In contrast, peaks

DOI:10.1063/1674-0068/cjcp1812293

d and b become stronger with longer trapping time of 45 ms. There must exist a higher excited state above the initial state of peaks d and b, which can decay to this initial state, and the lifetime of this initial state should be very long. According to the calculations of O'Malley and Beck, the lifetime of level $^3P_0$ is 2200 y [38]. Moreover, near the photodetachment threshold, the cross section of d-orbital photodetachment is usually two orders of magnitude lower than that of p-orbital photodetachment [36]. These two evidences favored the assignment of $^3P_0$ to be the initial state of peaks b and d. Peaks h and f should be transitions coming from $^3F_2$ not $^3F_3$ in that the J of their final states are 5/2 and 3/2, respectively. According to the transition rules of photodetachment, the smaller change of J before and after detachment is, the higher the transition possibility will be [39]. All these conclusions discussed above are illustrated in FIG. 3. The colors of vertical sticks in FIG. 2 indicate three different bound states of Lu^-.

The energy calibrations were done by using the well-known transitions of rhenium anions Re^-. To compensate the slightly nonlinear behavior between E_k and r^2 in a larger kinetic energy range, the following equation is used to convert the spectra versus the radius r to the kinetic energy E_k,

$$E_k = \alpha_2 r^2 + \alpha_4 r^4 \quad (2)$$

where the coefficients α_2 and α_4 were determined by the least squares method, as shown in FIG. 4. Since all the binding energies of transitions originated from the ground state of Lu^- fall out of the tuning range of our dye laser, we cannot scan a suitable transition slightly above its threshold to accurately measure the electron affinity. Since the kinetic energy of peak a is much smaller than that of peak g, peak a is chosen to determine the EA value. To determine the binding energy of peak a as accurate as possible, a local linear interpolation method is used as described by the following equation

$$E_k = E_{k0} + \alpha_2(r^2 - {r_0}^2) \quad (3)$$

Here E_k is the kinetic energy and r is the radius of the peak to be determined, and E_{k0} and r_0 correspond to the chosen transitions of Re^-. α_2 is still the calibration coefficient before the term r^2. The photon energy $h\nu$ is tuned so that r is as close to r_0 as possible. Since E_{k0} is accurately known, Eq.(3) leads to a smaller error compared with Eq.(2) for $r \approx r_0$.

The binding energy of peak a is measured to be 9402.6(50) cm^{-1}. The final state of transition a, Lu ($6s^26p$) $^2P_{3/2}$, is 7476.39 cm^{-1} above the ground state of Lu [37]. Thus, the EA of Lu is determined to be 1926.2±5.0 cm^{-1} or 0.23882(62) eV by subtracting 7476.39 cm^{-1} from 9402.6(50) cm^{-1}. Note that 1 eV=8065.544005(50) cm^{-1}, as recommended by 2014 CODATA [40]. This value is not consistent with the experimental result reported by Davis and Thompson mainly due to their lower energy resolution and

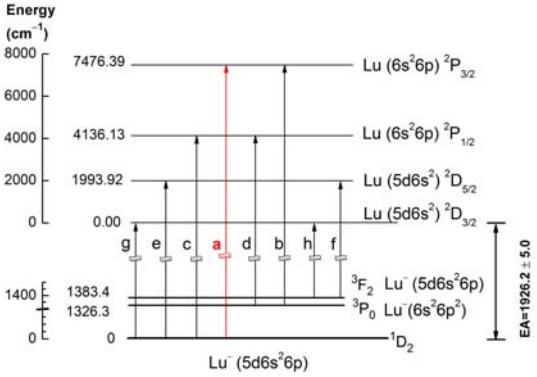

FIG. 3 Energy levels of Lu and Lu^- related to the present measurement. The labels of each transition are the indexes of the observed peaks in FIG. 2. The transition a, $Lu(^2P_{3/2}) \leftarrow Lu^-(^1D_2)$, is used for the electron affinity measurement.

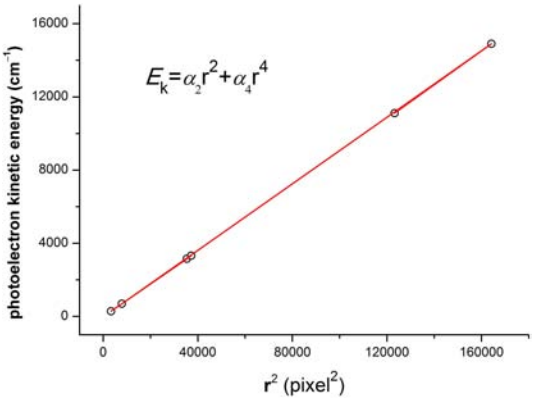

FIG. 4 Energy calibrations using rhenium anions Re^-. The open circles are experimental data.

lower signal-to-noise ratio. The two excited energy levels of Lu^- can be obtained through peaks d, b, h, and f, which are determined as 1326.3(70) and 1383.4(70) cm^{-1} above the ground state, respectively. So far, the binding energies of the eight observed peaks can all be settled down combined with the data of energy levels of Lu. All these have been summarized in Tables I, II and illustrated in FIG. 3.

FIG. 5 shows the binding energy spectrum of LuO^- at temperature 15 K with trapping time of 45 ms. The three sharp peaks correspond to the Lu−O stretch vibrational progressions. The EA and vibrational frequency was measured to be 13108(74) and 827(77) cm^{-1} respectively. The thermal broadening related to molecule anionic species was significantly reduced. This demonstrates that cryo-SEVI method is a powerful tool for investigating the complicated electronic structures of lanthanides.

DOI:10.1063/1674-0068/cjcp1812293

TABLE I Measured binding energies and asymmetry parameters of Lu^-.

Peaks	Levels (Lu←Lu^-)	Binding energy/cm^{-1}	β
a	$^2P_{3/2}$ ($6s^26p$)←$^1D_2$ ($5d6s^26p$)	9402.6(50)	−0.43
b	$^2P_{3/2}$ ($6s^26p$)←$^3P_0$ ($6s^26p^2$)	8076.3(70)	−0.66
c	$^2P_{1/2}$ ($6s^26p$)←$^1D_2$ ($5d6s^26p$)	6062.3(50)*	−0.71
d	$^2P_{1/2}$ ($6s^26p$)←$^3P_0$ ($6s^26p^2$)	4736(12)	0.25
e	$^2D_{5/2}$ ($5d6s^2$)←$^1D_2$ ($5d6s^26p$)	3920.1(50)*	0.86
f	$^2D_{5/2}$ ($5d6s^2$)←$^3F_2$ ($5d6s^26p$)	2537(12)	0.49
g	$^2D_{3/2}$ ($5d6s^2$)←$^1D_2$ ($5d6s^26p$)	1916(10)	0.81
h	$^2D_{3/2}$ ($5d6s^2$)←$^3F_2$ ($5d6s^26p$)	543(12)	0.65

* These values are extracted by using the energy intervals of Lu and the related measured transitions.

TABLE II Measured fine structures of Lu^- and the summary of all the electron affinity results of Lu.

	Levels	Energy/cm^{-1}
Fine structures of Lu^-	$^3P_0$←$^1D_2$	1326.3(70)
in this work	$^3F_2$←$^1D_2$	1383.4(70)
	Electron affinity value	Reference
The summary of	0.353 eV	Calculated [15]
all the electron	0.329 eV	Calculated [14]
affinity results of Lu	0.190 eV	Calculated [10]
	0.257 eV	Calculated [11]
	2706 cm^{-1}	Calculated [12]
	2665 cm^{-1}	Calculated [13]
	0.34 (1) eV	Measured [9]
	0.23882 (62) eV or 1926.2 (50) cm^{-1}	This work (measured)

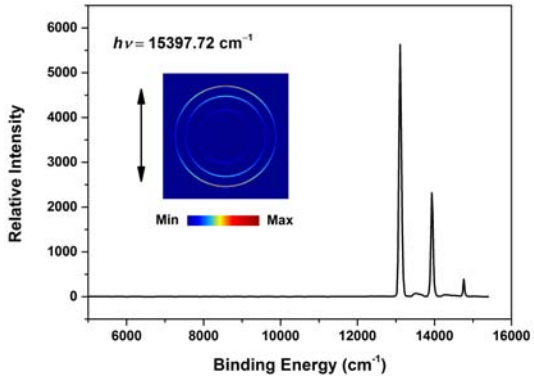

FIG. 5 The photoelectron image and the binding energy spectrum of LuO^- at photon energy $h\nu$=15397.72 cm^{-1} with the trapping time 45 ms and the temperature 15 K.

IV. CONCLUSION

In brief, the high resolution photoelectron spectra of Lu^- and LuO^- have been obtained through our newly-built cryo-SEVI apparatus. The electron affinity of Lu^- was measured to be 1926.2(50) cm^{-1} or 0.23882(62) eV. Two excited states of Lu^-, $^3P_0$ and $^3F_2$ were observed, which were 1326.3(70) and 1383.4(70) cm^{-1} above the ground state of Lu^-, respectively. As demonstrated in the present work, this new apparatus has a distinct advantage over the traditional photoelectron spectroscopy. As we all know, electron affinities of most lanthanides still remain unknown. A plan to explore the electron affinities and structures of lanthanides via the cryo-SEVI method is being carried on in our group.

V. ACKNOWLEDGEMENTS

This work was supported by the National Natural Science Foundation of China (No.91736102) and the National Key R&D program of China (No.2018YFA0306504).

[1] J. C. Rienstra-Kiracofe, G. S. Tschumper, and H. F. Schaefer III, Chem. Rev. **102**, 231 (2002).
[2] T. Andersen, Phys. Rep. **394**, 157 (2004).

DOI:10.1063/1674-0068/cjcp1812293

[3] T. Andersen, H. K. Haugen, and H. Hotop, J. Chem. Phys. Ref. Data **28**, 1511 (1999).
[4] M. Scheer, R. C. Bilodeau, C. A. Brodie, and H. K. Haugen, Phys. Rev. A **58**, 2844 (1998).
[5] M. Vandevraye, C. Drag, and C. Blondel, Phys. Rev. A **85**, 612 (2012)
[6] H. Hotop and W. C. Lineberger, J. Phys. Chem. Ref. Data **4**, 539 (1975).
[7] R. Middleton, *A Negative-Ion Cookbook*, Philadelphia: University of Pennsylvania Press, (1990).
[8] Y. Saitoh, B. Yotsombat, K. Mizuhashi, and S. Tajima, Rev. Sci. Instrum. **71**, 955 (2000).
[9] V. T. Davis and J. S. Thompson, J. Phys. B: At. Mol. Opt. Phys. **34**, L433 (2001).
[10] S. H. Vosko and J. A. Chevary, J. Phys. B: At. Mol. Opt. Phys. **26**, 873 (1993).
[11] E. Eliav, U. Kaldor, and Y. Ishikawa, Phys. Rev. A **52**, 291 (1995).
[12] A. Borschevsky. E. Eliav, M. J. Vilkas, Y. Ishikawa, and U. Kaldor, Eur. Phys. J. D **45**, 115 (2007).
[13] B. Karaçoban and L. Özdemir, Chin. J. Phys. **50**, 40 (2011).
[14] S. M. O'Malley and D. R. Beck, J. Phys. B **33**, 4337 (2000).
[15] S. M. O'Malley and D. R. Beck, Phys. Rev. A **79**, 012511 (2009).
[16] X. B. Wang and L. S. Wang, Rev. Sci. Instrum. **79**, 073108 (2008).
[17] C. Hock, J. B. Kim, M. L.Weichman, T. I. Yacovitch, and D. M. Neumark, J. Chem. Phys. **137**, 244201 (2012).
[18] A. Osterwalder, M. J. Nee, J. Zhou, and D. M. Neumark, J. Chem. Phys. **121**, 6317 (2004).
[19] I. Le'on, Z. Yang, H. T. Liu, and L. S. Wang, Rev. Sci. Instrum. **85**, 083106 (2014).
[20] J. B. Kim, M. L. Weichman, T. F. Sjolander, D. M. Neumark, J. Klos, M. H. Alexander, and D. E. Manolopoulos, Science **349**, 510 (2015).
[21] H. T. Liu, C. G. Ning, D. L. Huang, P. D. Dau, and L. S. Wang, Angew. Chem. Int. Ed. **53**, 2464 (2014).
[22] H. T. Liu, C. G. Ning, D. L. Huang, and L. S. Wang, Angew. Chem. Int. Ed. **52**, 8976 (2013).
[23] X. L. Chen and C. G. Ning, J. Chem. Phys. **145**, 084303 (2016).
[24] X. L. Chen, Z. H. Luo, J. M. Li, and C. G. Ning, Sci. Rep. **6**, 24996 (2016).
[25] X. L. Chen and C. G. Ning, J. Phys. Chem. Lett. **8**, 2735 (2017).
[26] R. L. Tang, X. L. Chen, X. X. Fu, H. Wang, and C. G. Ning, Phys. Rev. A **98**, 020501(R) (2018).
[27] R. L. Tang, X. X. Fu, and C. G. Ning, J. Chem. Phys. **149**, 134304 (2018).
[28] X. L. Chen and C. G. Ning, Phys. Rev. A **93**, 052508 (2016).
[29] X. X. Fu, Z. H. Luo, X. L. Chen, J. M. Li, and C. G. Ning, J. Chem. Phys. **145**, 164307 (2016).
[30] Z. H. Luo, X. L. Chen, J. M. Li, and C. G. Ning, Phys. Rev. A **93**, 020501(R) (2016).
[31] X. X. Fu, J. M. Li, Z. H. Luo, X. L. Chen, and C. G. Ning, J. Chem. Phys. **147**, 064306 (2017).
[32] A. T. J. B. Eppink and D. H. Parker, Rev. Sci. Instrum. **68**, 3477 (1997).
[33] W. C. Wiley and I. H. McLaren, Rev. Sci. Instrum. **26**, 1150 (1955).
[34] B. Dick, Phys. Chem. Chem. Phys. **16**, 570 (2014).
[35] J. Cooper and R. N. Zare, J. Chem. Phys. **48**, 942 (1968).
[36] Y. Liu and C. G. Ning, J. Chem. Phys. **143**, 144310 (2015).
[37] J. E. Sansonetti and W. C. Martin, J. Phys. Chem. Ref. Data **34**, 1559 (2005).
[38] S. M. O'Malley and D. R. Beck, Phys. Rev. A **81**, 032503 (2010).
[39] M. Scheer, C. A. Brodie. R. C. Bilodean, and H. K. Haugen, Phys. Rev. A **58**, 2051 (1998).
[40] P. J. Mohr, D. B. Newell, and B. N. Taylor, Rev. Mod. Phys. **88**, 035009 (2016).

DOI:10.1063/1674-0068/cjcp1812293